Journal of Solid State Chemistry **156,** 437–444 (2001)
doi:10.1006/jssc.2000.9019, available online at http://www.idealibrary.com on IDEAL®

Transport Properties and Thermal Expansion of $Sr_{0.97}Ti_{1-x}Fe_xO_{3-\delta}$ ($x = 0.2-0.8$)

V. V. Kharton,*,†,[1] A. V. Kovalevsky,* A. P. Viskup,* J. R. Jurado,‡ F. M. Figueiredo,†,§ E. N. Naumovich,* and J. R. Frade†

*Institute of Physicochemical Problems, Belarus State University, 14 Leningradskaya Str., 220080 Minsk, Republic of Belarus; †Department of Ceramics and Glass Engineering, UIMC, University of Aveiro, 3810-193 Aveiro, Portugal; ‡Institute of Ceramics and Glass, CSIC, 28500 Arganda del Rey, Madrid, Spain; and §Science & Technology Department, Universidade Aberta, R. Esc. Politecnica 147, 1269-001 Lisbon, Portugal

Received August 10, 2000; in revised form October 18, 2000; accepted October 27, 2000

Increasing iron concentration in perovskite-type solid solutions $Sr_{0.97}Ti_{1-x}Fe_xO_{3-\delta}$ ($x = 0.2-0.8$) was found to decrease the unit cell volume and to increase the partial ionic and electronic conductivities as well as the thermal expansion. The oxygen permeation through $Sr_{0.97}(Ti,Fe)O_{3-\delta}$ membranes is limited by both bulk ionic conduction and surface exchange rates. Prolonged stabilization under oxygen chemical potential gradients suggests formation of ordered microdomains in the perovskite lattice. The activation energy for the ionic conductivity, evaluated from oxygen permeation and Faradaic efficiency data, is nearly independent of iron content, varying in the range 97–104 kJ/mol. Thermal expansion coefficients of $Sr_{0.97}Ti_{1-x}Fe_xO_{3-\delta}$ ($x = 0.4-0.8$) vary from $(11.7-13.8)\times10^{-6}$ K^{-1} at temperatures of 300–720 K to $(16.6-27.0)\times10^{-6}$ K^{-1} at higher temperatures. In comparison with the Sr(Ti, Co)$O_{3-\delta}$ system, strontium titanates ferrites possess somewhat poorer transport properties, but lower thermal expansion. © 2001 Academic Press

Key Words: **perovskites; oxygen permeation; faradaic efficiency; ionic conductivity; strontium titanate–ferrite; thermal expansion; mpixed conductors.**

INTRODUCTION

Mixed conducting oxides with ABO_3 perovskite structure are of considerable interest for applications in high-temperature electrochemical systems, such as ceramic membranes for oxygen separation and partial oxidation of hydrocarbons, electrodes of solid oxide fuel cells (SOFCs), and sensors (1–5). Among known perovskite-like mixed conductors, the highest oxygen ionic conductivity is observed in materials based on strontium cobaltite, $SrCoO_{3-\delta}$, and strontium ferrite, $SrFeO_{3-\delta}$ (4–8). However, these oxides exhibit a number of specific disadvantages, including thermodynamic and dimensional instability under high oxygen chemical potential gradients and reactivity with gas species such as CO_2 (9–13). Substitution of cobalt or iron with higher valence metal cations such as Ti or Cr may improve the stability in reducing environments (8), and a moderate A site cation deficiency is useful in order to enhance the stability of these perovskites in CO_2-containing atmospheres (10, 12).

An increase in the oxygen ionic transport has been observed when doping with moderate amounts of higher valence cations in the B sublattice (14, 15). This effect is associated with a possible stabilization of the cubic perovskite structure, which provides better geometrical abilities for ion hopping in comparison with various ordered or distorted perovskite phases (4, 5, 15). Also, both the ionic conductivity and the oxygen surface exchange coefficient are complex functions of the concentration of oxygen ion vacancies, and often show a maximum in a certain concentration. An appropriate cation doping enables an optimization of the transport properties for given external conditions. In particular, at oxygen partial pressures close to 20 kPa the maximum ionic conductivity in the systems $SrCo_{1-x}Ti_xO_{3-\delta}$ and $SrCo_{1-x}Fe_xO_{3-\delta}$ is observed for x values in the ranges 0.05–0.20 and 0.20–0.35, respectively (5, 14–16). Oxygen permeation through dense ceramic membranes of $SrCoO_{3-\delta}$- and $SrFeO_{3-\delta}$-based solid solutions is limited by both bulk ionic transport and oxygen surface exchange and may thus be improved by surface modification of oxide ceramics (15, 17, 18).

The emphasis of the present work is on the system $Sr_{0.97}Ti_{1-x}Fe_xO_{3-\delta}$ ($x = 0.2$–0.8); this continues our studies of the $SrCoO_{3-\delta}$- and $SrFeO_{3-\delta}$-based phases as potential materials for electrochemical applications (5, 11, 12, 14–21). Particular attention is given to the oxygen ionic transport and thermal expansion, which determine the applicability of these perovskites in high-temperature electrochemical cells.

[1] To whom correspondence should be addressed at Department of Ceramics and Glass Engineering, UIMC, University of Aveiro, 3810-193 Aveiro, Portugal. Fax: +351-234-425300. E-mail: kharton@cv.ua.pt or kharton@hp.bsu.unibel.by.

0022-4596/01 $35.00

EXPERIMENTAL

Solid-state synthesis of $Sr_{0.97}Ti_{1-x}Fe_xO_{3-\delta}$ ($x = 0.2$–0.8) powders was carried out by a standard ceramic technique. Mixtures of high-purity binary metal oxides and salts were fired at 1270–1420 K in air for 15–35 h with multiple intermediate regrindings. Samples were pressed at 300–500 MPa in the shape of bars ($4 \times 4 \times 30$ mm^3), and disks of various thickness (diameter, 10 to 20 mm), and then sintered in air at 1520–1720 K, during 8–20 h, to obtain gas-tight ceramics. The density of the ceramics, measured by the standard pycnometric procedure, was higher than 92% of the theoretical density; the theoretical density was calculated using the unit cell parameters (Fig. 1) determined by refinement of X-ray diffraction (XRD) patterns. After sintering, the samples were annealed in air at 1170 K for 5–10 h with subsequent slow cooling, in order to obtain oxygen nonstoichiometry close to equilibrium at room temperature. Only ceramic samples that had their gas tightness verified previously were used for the oxygen permeation and Faradaic efficiency measurements.

The prepared materials were characterized using XRD, X-ray fluorescence analysis (XFA), emission spectroscopic analysis, infrared (IR) absorption spectroscopy, dilatometry, and measurements of electrical conductivity, oxygen permeability, and Faradaic efficiency. The experimental procedures used for the characterization were described in detail elsewhere (14–23). Deviations in the cation composition of the studied ceramics from the formula compositions were determined to be less than 0.2 at.%. The total impurity content was less than 0.05 at.%, which is close to the sensitivity limits of the analytical techniques used. The dilatometric measurements were performed with a heating rate of 3.0 ± 0.5 K/min. For all the oxygen permeability and Faradaic efficiency results presented in this paper, the membrane feed-side oxygen partial pressure (p_2) was maintained at 21 kPa (atmospheric air). The oxygen partial pressure at the membrane permeate side (p_1) varied from 0.1 Pa to 21 kPa, as determined by the electromotive force (emf, E) reading of a potentiometric oxygen sensor, using the Nernst equation:

$$E = \frac{RT}{4F} \cdot \ln\left(\frac{p_2}{p_1}\right). \qquad [1]$$

When analyzing the permeation processes, we use hereafter the quantities of the oxygen permeation flux density j (mol $\times$ s^{-1} $\times$ cm^{-2}) and specific oxygen permeability $J(O_2)$ (mol $\times$ s^{-1} $\times$ cm^{-1}) defined as (24)

$$J(O_2) = j \cdot d \cdot \left[\ln \frac{p_2}{p_1}\right]^{-1}, \qquad [2]$$

where d is the membrane thickness. The quantity $J(O_2)$ is suitable to identify a limiting effect of surface exchange rate on the oxygen permeation on the basis of membrane thickness dependencies of the permeation fluxes (15). This quantity is, by definition, proportional to $j \times d$ and should thus be independent of thickness in the case when surface limitations are negligible. In this situation, $J(O_2)$ is proportional to so-called ambipolar conductivity (σ_{amb}), averaged for a given oxygen partial pressure range,

$$J(O_2) = \frac{RT}{16F^2} \cdot \overline{\sigma_{amb}} = \frac{RT}{16F^2} \cdot \overline{\frac{\sigma_o \cdot \sigma_e}{\sigma_o + \sigma_e}} = \frac{RT}{16F^2} \cdot \overline{\sigma \cdot t_o(1 - t_o)}, \qquad [3]$$

where t_o is the oxygen ion transference number, and σ, σ_o, and σ_e are the total, oxygen ionic, and electronic conductivities, respectively. When oxygen exchange limitations are considerable, $J(O_2)$ should increase with increasing membrane thickness for a given oxygen chemical potential gradient, due to a decreasing role of the surface exchange.

The Faradaic efficiency technique was described elsewhere (18, 20). The sample is hermetically sealed onto a solid electrolyte cell equipped with an oxygen pump and an oxygen sensor. A given current I_{pump} is then supplied to the

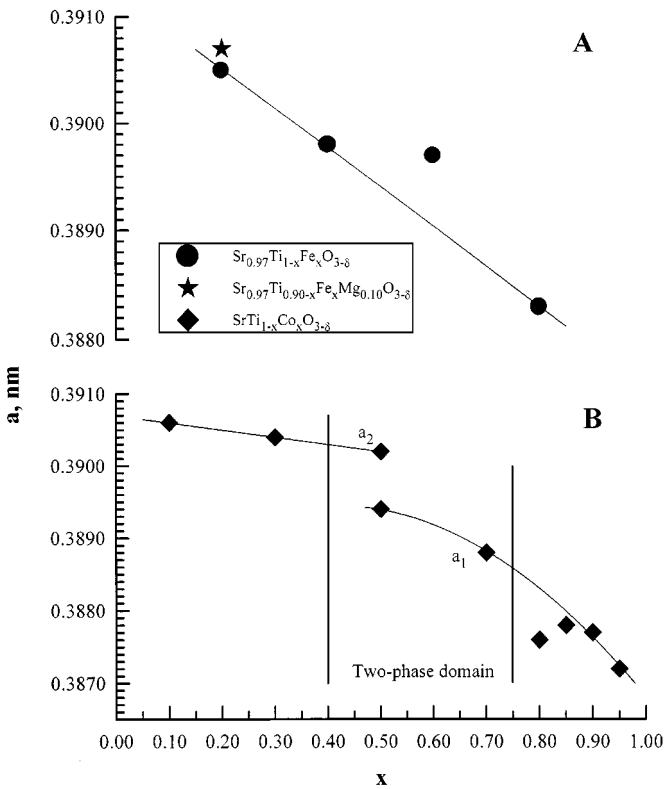

FIG. 1. Composition dependence of the cubic perovskite unit cell parameter in the $Sr_{0.97}Ti_{1-x}Fe_xO_{3-\delta}$ (A) and $SrTi_{1-x}Co_xO_{3-\delta}$ (B) systems. The error in the lattice parameter determination is ± 0.0001 nm.

pump, lowering the oxygen content inside the cell, and the current through the sample I_{sample} is adjusted to obtain a suitable time-independent emf value in the sensor under steady state conditions. The ion transference number is then obtained from the ratio $[(I_{pump} - 4FJ)/I_{sample}]$, where J corresponds to the permeation flux, determined separately before each Faradaic efficiency test, under identical conditions of temperature and p_1.

RESULTS AND DISCUSSION

1. Structure

XRD analysis of the $Sr_{0.97}Ti_{1-x}Fe_xO_{3-\delta}$ samples showed formation of a single cubic perovskite phase, with the unit cell parameter given in Fig. 1. For comparison, Fig. 1 also shows the XRD data for $SrTi_{1-x}Co_xO_{3-\delta}$ (15, 16) and $Sr_{0.97}Ti_{0.7}Fe_{0.2}Mg_{0.1}O_{3-\delta}$ (18). The unit cell volume of $Sr_{0.97}$(Ti, Fe)$O_{3-\delta}$ decreases with increasing x, in agreement with the literature data (25). This suggests that trivalent Fe cations in the high-spin state, typical for the perovskite-type ferrites (26), exist in the lattice mainly in tetrahedral coordination; presence of a part of iron cations as octahedrally coordinated Fe^{4+} is also probable. In both cases, the radii of iron cations are less than those of Ti^{4+}, while ionic radii of Fe^{3+} in the octahedral coordination are larger compared to those of tetravalent titanium (27). Most probably, decreasing oxygen content with increasing x may not be suggested as a reason for the observed changes in the unit cell parameter, since reducing oxygen concentration in perovskite oxides leads, as a rule, to the lattice expansion (for example, Refs. 28 and 29). Doping with magnesium leads to increasing unit cell volume, as expected from the Mg^{2+} size (27).

It should be mentioned that existence of a significant fraction of Fe^{3+} cations in tetrahedral coordination should lead to formation of ordered brownmillerite-like microdomains, as reported for $SrFeO_{3-\delta}$- and $CaFeO_{2.5\pm\delta}$-based systems (30, 31). Indeed, Steinvik *et al.* (25) reported ordering in the lattice of $SrTi_{1-x}Fe_xO_{3-\delta}$ phases at $x > 0.5$. The discontinuity of the composition dependence of the unit cell parameter of $Sr_{0.97}Ti_{1-x}Fe_xO_{3-\delta}$ at $x = 0.6$ (Fig. 1) confirms this assumption. A clear evidence of the ordering phenomena in the title materials was also obtained from the data on oxygen ionic transport discussed below.

In general, the dependence of the unit cell parameter on composition in the $SrTi_{1-x}Co_xO_{3-\delta}$ system is close to that in $Sr_{0.97}$(Ti, Fe)$O_{3-\delta}$. However, in the cobalt-containing system two cubic perovskite phases co-exist in the intermediate composition range; their lattice parameters are marked as a_1 and a_2 in Fig. 1. The nonlinear dependence of the unit cell dimensions on x at high cobalt content in $SrTi_{1-x}Co_xO_{3-\delta}$ may also indicate ordering in these oxides.

2. Electronic Conductivity

The temperature dependence of the total electrical conductivity of $Sr_{0.97}$(Ti, Fe)$O_{3-\delta}$ solid solutions in air is shown in Fig. 2. Increasing iron content leads to a drastic increase in conductivity that is predominantly electronic (Fig. 3), because the ion transference numbers of these materials are less than 0.1. Increasing electronic conduction is most probably associated with progressive delocalization of atomic levels and increasing bandwidth. Such an assumption is attested by the decrease in activation energy for electronic transport and the decrease in temperature of the transition from semiconductor to metallic-like behavior with increasing iron concentration. The activation energy (E_a) for the electronic conductivity, given in Fig. 4, was calculated using the standard Arrhenius law

$$\sigma = \frac{A_0}{T} \cdot \exp\left(-\frac{E_a}{RT}\right), \qquad [4]$$

where A_0 is the preexponential factor.

One should mention the hypothesis (24) that the decrease in conductivity of $SrFeO_{3-\delta}$ in the high-temperature region is due to oxygen losses, resulting in a decrease in electron hole concentration. However, this seems to be contradicted

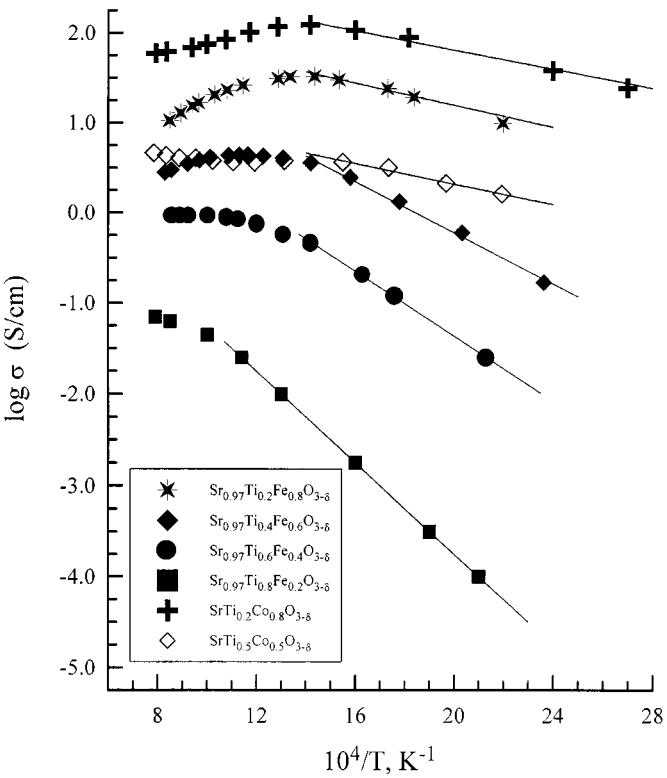

FIG. 2. Temperature dependence of the total electrical conductivity of $Sr_{0.97}$(Ti, Fe)$O_{3-\delta}$ solid solutions in air.

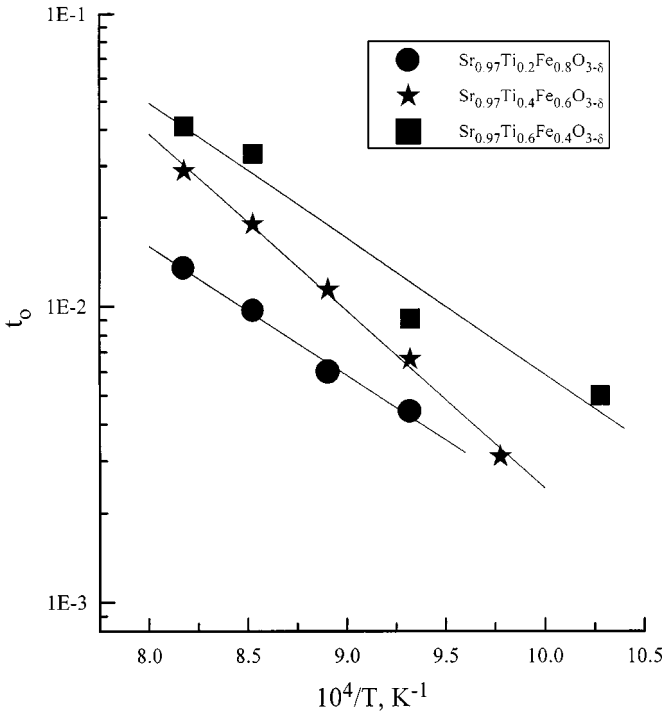

FIG. 3. Temperature dependence of the oxygen ion transference numbers in air determined by the Faradaic efficiency measurements.

by X-ray absorption spectroscopy data of strontium ferrite (26). The Co-containing perovskites exhibit a behavior similar to that of Fe-containing phases, but the conductivity is significantly higher in the case of $SrCoO_{3-\delta}$-based materials (Fig. 2), in agreement with the properties of parent compounds (5, 21, 32).

3. Time Degradation of Oxygen Permeability

After being placed under an oxygen chemical potential gradient some of the tested $Sr_{0.97}Ti_{1-x}Fe_xO_{3-\delta}$ ceramic samples showed a prolonged transient regime before reaching steady state, as illustrated by Fig. 5. The initial time of stabilization was 50–500 h when an oxygen chemical potential gradient was first applied across the sample. Subsequent measurements required smaller but still significant transient times (in the range 3–40 h). Time independence of the oxygen pressure at the membrane permeate side during 20–40 h, under constant oxygen flux through the membrane, was thus used as a criterion for steady state attainment. All the results on oxygen permeation presented below were obtained under these conditions, except for the upper curve in Fig. 6, which corresponds to a pseudo-steady state, i.e., when the permeation flux appears to be approximately time independent.

More detailed studies are necessary to identify reasons for such transient behavior. Nevertheless, the obtained results indicate that the stabilization time is significantly shorter when the iron concentration is smaller (Fig. 5). In addition, the results obtained before and after degradation for about 500 h (Fig. 6) yield similar values of effective activation energy for oxygen permeation. The values of oxygen permeation decrease by a factor of about 2.5 after the degradation process.

The observed trends may be explained in terms of formation of ordered microdomains, as mentioned above. Increasing iron content should indeed result in larger ordered volume in the lattice if the degradation was due to association of oxygen vacancies and iron cations in brownmillerite-type domains, as found for strontium ferrite phases (30). Here, Fig. 5 suggests that the time necessary to form ordered domains should increase with x in $Sr_{0.97}Ti_{1-x}Fe_xO_{3-\delta}$. Furthermore, if the ionic charge carriers in the ordered part of the lattice are completely blocked, ordering should lead to a lower effective concentration of ionic charge carriers and, thus, a lower preexponential factor for the Arrhenius plots of ionic conductivity results after degradation (A_o in Eq. [4]). Local ordering may thus result in smaller oxygen transport parameters without considerable changes in the activation energy, in agreement with the observed trend (Fig. 6). One may also assume some degradation of the surface exchange rate by taking into account the well-known correlation between oxygen exchange rates and oxygen diffusion coefficients (33).

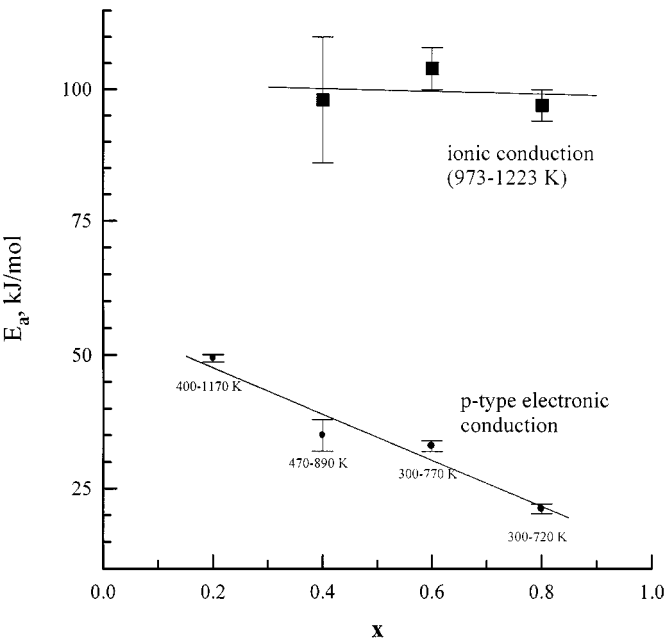

FIG. 4. Composition dependence of the activation energies for the ionic and electronic conductivities in the $Sr_{0.97}Ti_{1-x}Fe_xO_{3-\delta}$ system in air. The temperature ranges, marked under the points, correspond to the data taken for the calculations using the Arrhenius model.

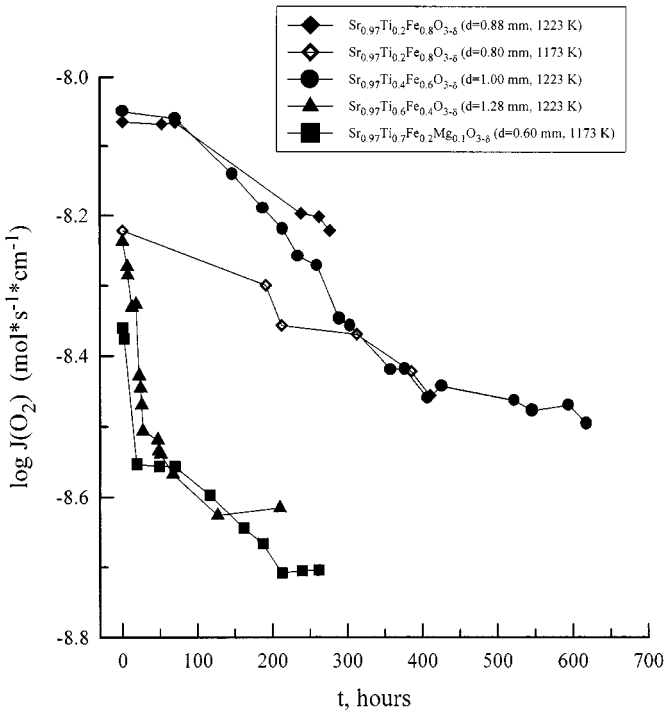

FIG. 5. Time dependence of specific oxygen permeability of $Sr_{0.97}Ti_{1-x}Fe_xO_{3-\delta}$ ceramics after placing membranes under fixed oxygen chemical potential gradient.

4. Surface Limitations of Oxygen Permeation

Figure 7A presents the dependence of the permeation flux density through some $Sr_{0.97}Ti_{1-x}Fe_xO_{3-\delta}$ membranes with varying thicknesses on oxygen pressure gradient, and the corresponding values of the oxygen permeability are shown in Fig. 7B. Increasing membrane thickness leads to decreasing permeation fluxes, while the $J(O_2)$ values are increasing. This unambiguously indicates nonnegligible surface exchange limitations to the oxygen transport, as discussed above. Such behavior is typical for $Sr_{0.97}Ti_{0.2}Fe_{0.8}O_{3-\delta}$ in the entire studied temperature range (970–1270 K). Decreasing iron content leads to a lower ionic conductivity and, hence, oxygen exchange is less likely to play a limiting role, especially at reduced temperatures. For the materials with $x = 0.4$–0.6, significant limitations of oxygen exchange limitations were found at $T > 1100$ K, whereas at lower temperatures the effect of interphase exchange is comparable to the experimental error. The behavior of strontium titanates ferrites with smaller iron content ($x \leq 0.4$) has been analyzed elsewhere (17, 18).

An important consequence of surface exchange limitations on the oxygen permeability of $Sr_{0.97}(Ti,Fe)O_{3-\delta}$ solid solutions is that the ionic conductivity values, which were calculated from permeation data, might be underestimated due to higher overall resistance to oxygen transport. An alternative technique of Faradaic efficiency was thus also used to verify those results. However, nonnegligible polarization resistance may also lead to predictions of ionic conductivity that are significantly lower than the true values (18, 20), and the ionic conduction parameters presented hereafter should thus be understood rather as estimations. Nevertheless, the observed trends should reflect the true behavior of the title materials, since the variations in the values of oxygen ionic conductivity determined by different methods, and for membranes of various thicknesses, are comparable with experimental errors of the measurement techniques (Fig. 8).

5. Ionic Conduction

The oxygen permeability of $Sr_{0.97}Ti_{1-x}Fe_xO_{3-\delta}$ ceramics increases regularly with increasing x (Fig. 9) due to increasing ionic and electronic conductivities. This is similar to a typical behavior for the $SrTi_{1-x}Co_xO_{3-\delta}$ system. However the oxygen transport is much faster in the later case, and Co-containing perovskites are thus more suitable for oxygen separation in oxidizing conditions. The data on oxygen permeation and total conductivity of $Sr_{0.97}(Ti, Fe)O_{3-\delta}$ were used to estimate the ion transference numbers and ionic conductivity using the

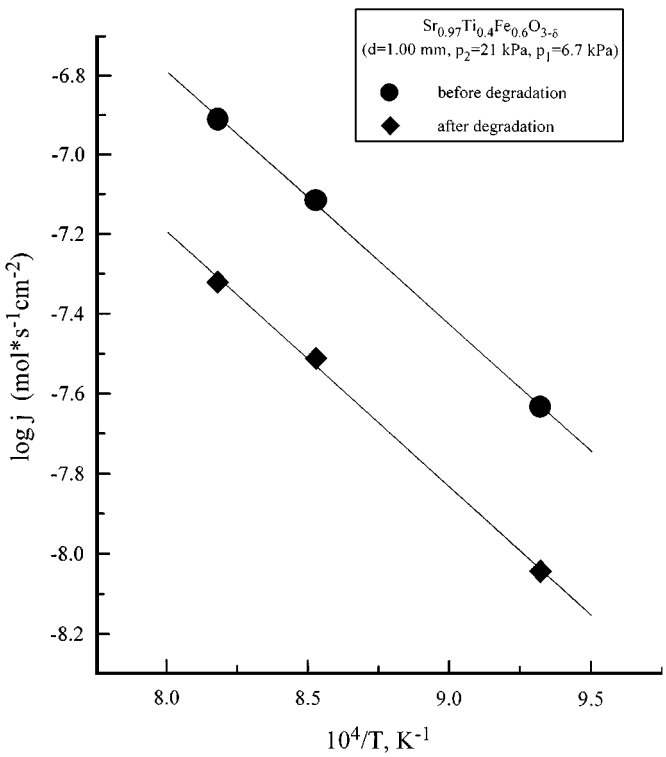

FIG. 6. Temperature dependence of the oxygen permeation flux density through $Sr_{0.97}Ti_{0.4}Fe_{0.6}O_{3-\delta}$ membrane before and after degradation (see text).

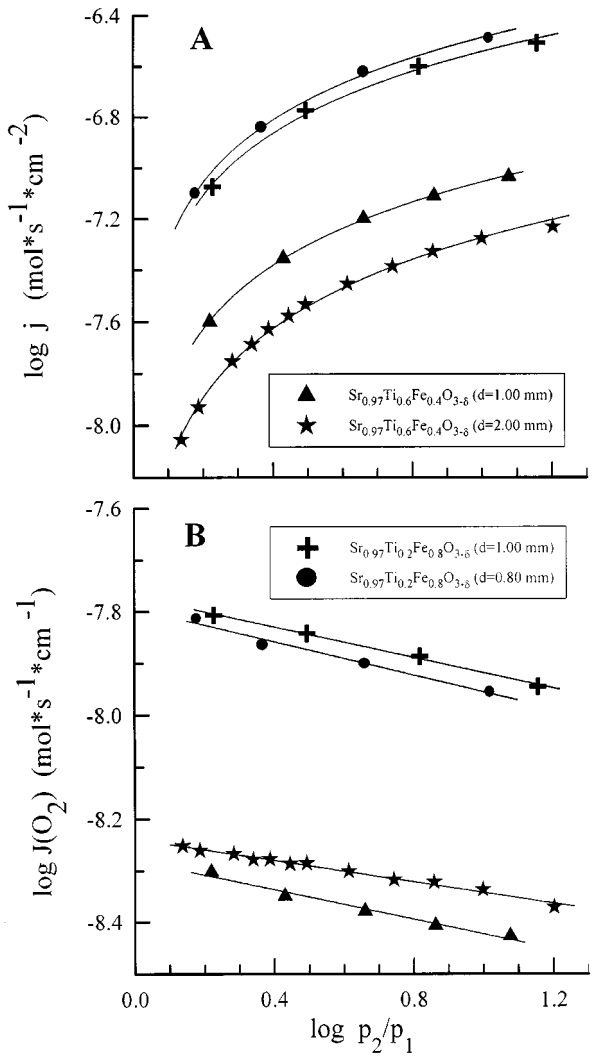

FIG. 7. Dependence of oxygen permeation flux density (A) and oxygen permeability (B) of $Sr_{0.97}Ti_{1-x}Fe_xO_{3-\delta}$ membranes on the oxygen partial pressure gradient at 1223 K ($p_2 = 21$ kPa).

relationships:

$$\overline{\sigma_{amb}} = 4Fd \cdot \left(\frac{\partial j}{\partial E}\right)_{E \to 0} \quad [5]$$

$$t_o = \frac{1}{2} - \frac{1}{2}\sqrt{1 - 4\frac{\overline{\sigma_{amb}}}{\sigma}}. \quad [6]$$

For materials with large iron concentrations ($x > 0.5$), these estimations are in relatively good agreement with the Faradaic efficiency data (Fig. 8). The ion transference numbers of $Sr_{0.97}Ti_{1-x}Fe_xO_{3-\delta}$ ($x = 0.6$–0.8) are in the range from 3×10^{-3} to 3×10^{-2} in atmospheric air and tend to decrease with reducing temperature (Fig. 3). For smaller iron contents, the experimental uncertainty is larger due to more significant effects of polarization resistance in the Faradaic efficiency cells and surface exchange limitations in the case of oxygen permeability experiments (18, 20). The estimated oxygen ion transference numbers of $Sr_{0.97}Ti_{1-x}Fe_xO_{3-\delta}$ with $x = 0.2$–0.4 are significantly higher (from 5×10^{-3} to 0.2). However, the activation energy for ionic conductivity of $Sr_{0.97}(Ti, Fe)O_{3-\delta}$ is nearly independent of iron content in the studied composition range, within the experimental error limits (Fig. 4), suggesting that ionic conduction is determined predominantly by the effective concentration of mobile charge carriers.

6. Thermal Expansion

Dilatometric curves of $Sr_{0.97}Ti_{1-x}Fe_xO_{3-\delta}$ ceramics can be approximated by two straight lines with a break at 650–800 K (Fig. 10). The drastic increase in the thermal expansion with increasing temperature is probably associated with oxygen losses in the course of heating (35, 36), leading to a greater oxygen vacancy concentration in the high temperature range. Another important factor, which also may lead to increasing thermal expansion at temperatures above 650 K, refers to disordering in the crystal lattice on heating. The observed correlation among oxygen nonstoichiometry, ionic conductivity, and thermal

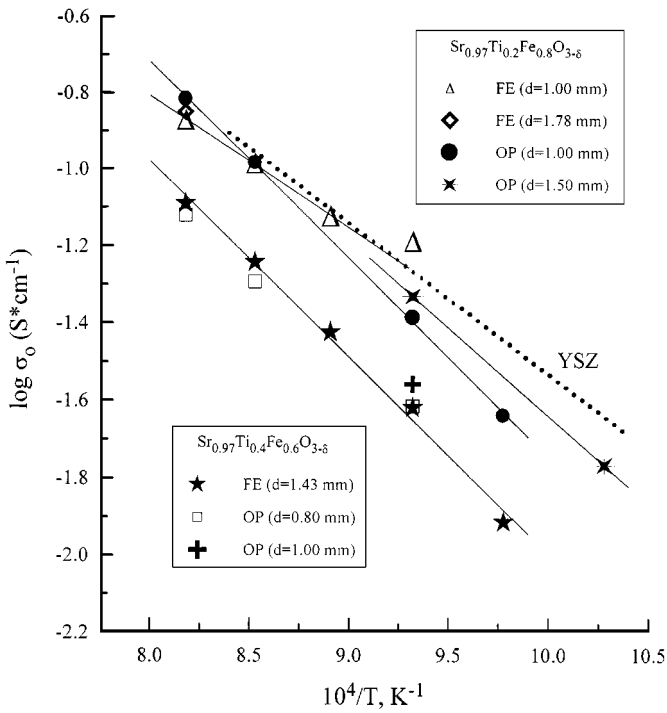

FIG. 8. Temperature dependence of oxygen ionic conductivity of $Sr_{0.97}Ti_{1-x}Fe_xO_{3-\delta}$ in air, calculated from the results of oxygen permeation (OP) and Faradaic efficiency (FE) measurements. The data on $Zr_{0.92}Y_{0.08}O_{1.96}$ solid electrolyte (YSZ), taken from Ref. (32), are shown for comparison.

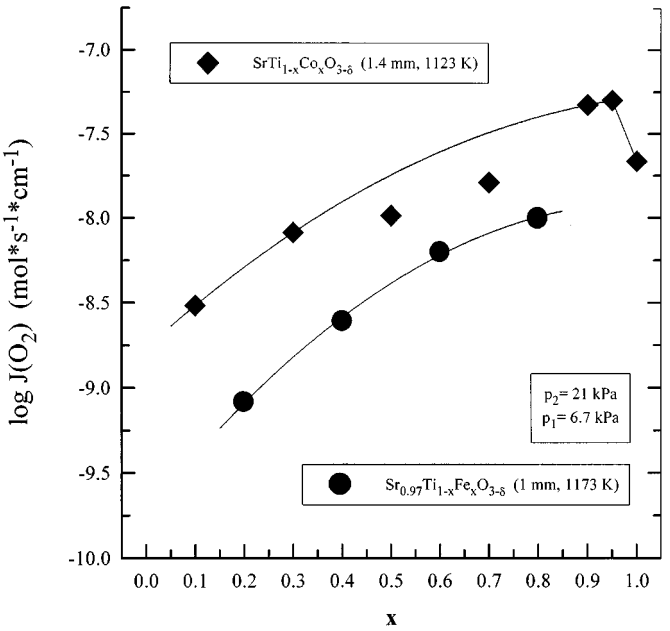

FIG. 9. Composition dependence of the oxygen permeability of $Sr_{0.97}Ti_{1-x}Fe_xO_{3-\delta}$ and $SrTi_{1-x}Co_xO_{3-\delta}$ under the fixed oxygen chemical potential gradient.

expansion confirms these statements. Figure 11 shows the dependence of thermal expansion coefficients (TECs), averaged in the two temperature ranges, on cation composition of the solid solutions $Sr_{0.97}Ti_{1-x}Fe_xO_{3-\delta}$ and $SrTi_{1-x}Co_xO_{3-\delta}$. These systems exhibit a similar behavior,

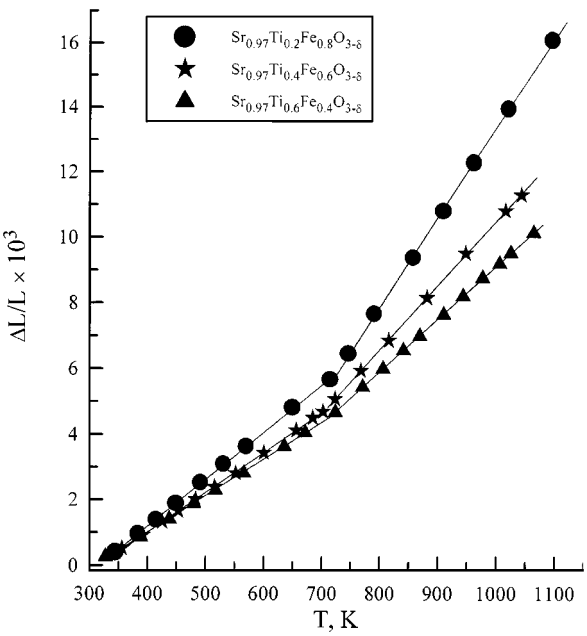

FIG. 10. Temperature dependence of relative elongation of $Sr_{0.97}Ti_{1-x}Fe_xO_{3-\delta}$ ceramics in air.

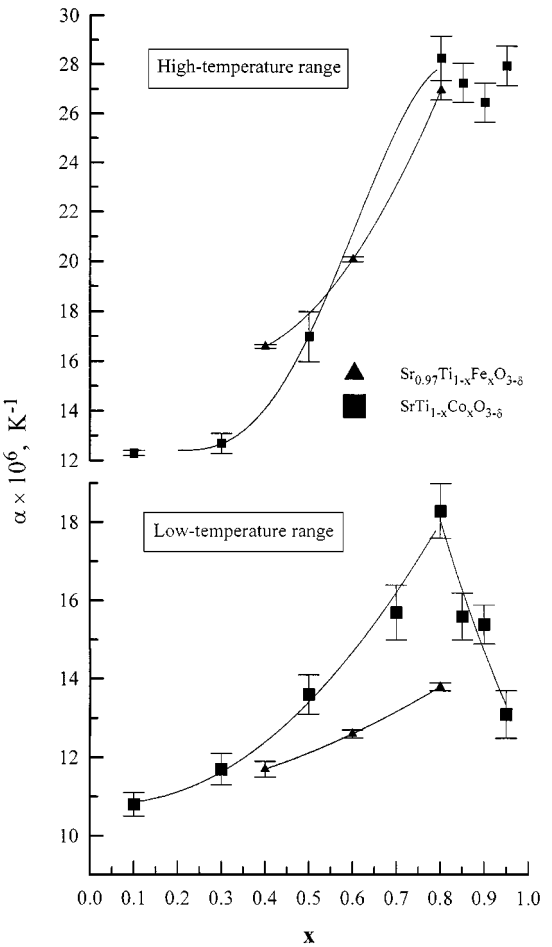

FIG. 11. Composition dependence of the average thermal expansion coefficients of $Sr_{0.97}Ti_{1-x}Fe_xO_{3-\delta}$ and $SrTi_{1-x}Co_xO_{3-\delta}$ ceramics in air.

but the Co-containing perovskites possess higher TEC values. Again, this may be explained in terms of oxygen vacancy concentration, since the average oxidation state of cobalt cations in these perovskites is typically lower than that of iron (see (5, 35, 37) and references therein).

CONCLUSION

Dense single-phase $Sr_{0.97}Ti_{1-x}Fe_xO_{3-\delta}$ ($x = 0.2$–0.8) samples were prepared by a standard ceramic technique and studied using X-ray diffraction, dilatometry, and measurements of the total electrical conductivity, oxygen permeation, and Faradaic efficiency. Increasing iron concentration in the perovskite-type solid solution decreases the cubic unit cell volume and increases the partial ionic and electronic conductivities. Oxygen permeation fluxes through $Sr_{0.97}(Ti, Fe)O_{3-\delta}$ membranes is limited by both bulk ionic conduction and surface exchange rates. Prolonged stabilization processes, observed after placing membranes under oxygen chemical potential gradient, suggest

possible formation of ordered microdomains in the perovskite lattice. The activation energy for ionic conductivity in the studied composition range is essentially independent of iron content, varying from 97 to 104 kJ/mol. Thermal expansion coefficients of $Sr_{0.97}Ti_{1-x}Fe_xO_{3-\delta}$ ($x = 0.4$–0.8) ceramics in air are in the range $(11.7–13.8) \times 10^{-6}\,K^{-1}$ at 300–720 K and $(16.6–27.0) \times 10^{-6}\,K^{-1}$ at 300–720 K; increasing iron content results in greater TEC values. The high thermal expansion hampers compatibility of strontium titanates ferrites with other materials in high-temperature electrochemical cells.

ACKNOWLEDGMENTS

This research was partially supported by FCT (Portugal), under Contract PRAXIS/P/CTM/14170/1998, by the Belarus Foundation for Basic Research, and by the Belarus Ministry of Education and Science.

REFERENCES

1. K. Kinoshita, "Electrochemical Oxygen Technology." Wiley, New York, 1992.
2. H. J. M. Bouwmeester and A. J. Burgraaf, *in* "Fundamentals of Inorganic Membrane Science and Technology" (A. J. Burgraaf and L. Cot, Eds.), p. 435. Elsevier, Amsterdam, 1996.
3. B. C. H. Steele, *in* "Proceedings of the 1st European SOFC Forum" (U. Bossel, Ed.), Vol. 1, p. 375. Lucerne, Switzerland, 1994.
4. Y. Teraoka, H.-M. Zhang, S. Furukawa, and N. Yamazoe, *Chem. Lett*. No. **11,** 1743 (1985).
5. V. V. Kharton, A. A. Yaremchenko, and E. N. Naumovich, *J. Solid State Electrochem.* **3,** 303 (1999).
6. R. M. Thorogood, R. Srinivasan, T. F. Yu, and M. P. Drake, U.S. Patent 5,240,480 (1993).
7. M. Schwartz, J. H. White, and A. F. Sammells, Int. Patent Application PCT/US96/14841 (1996), Publication No. WO 97/41060.
8. T. J. Mazanec, T. L. Cable, J. G. Frye, and W. R. Kliewer, U.S. Patent 5,744,015 (1998).
9. S. Pei, M. S. Kleevisch, T. P. Kobylinski, J. Faber, C. A. Udovich, V. Zhang-McCoy, B. D. Dabrowski, U. Balachandran, R. L. Mieville, and R. B. Poeppel, *Catal. Lett*. **30,** 201 (1995).
10. M. F. Carolan, P. N. Dyer, S. A. Motika, and P. B. Alba, U.S. Patent 5,712,220 (1998).
11. V. V. Kharton, A. A. Yaremchenko, A. V. Kovalevsky, A. P. Viskup, E. N. Naumovich, and P. F. Kerko, *J. Membr. Sci.* **163,** 307 (1999).
12. J. R. Jurado, F. M. Figueiredo, B. Charbage, and J. R. Frade, *Solid State Ionics* **118,** 89 (1999).
13. Q. Ming, M. D. Nersesyan, A. Wagner, J. Ritchie, J. T. Richardson, D. Luss, A. J. Jacobson, and Y. L. Yang, *Solid State Ionics* **122,** 113 (1999).
14. V. V. Kharton, E. N. Naumovich, and A. V. Nikolaev, *Solid State Phenomena* **39–40,** 147 (1994).
15. V. V. Kharton, Li Shuangbao, A. V. Kovalevsky, and E. N. Naumovich, *Solid State Ionics* **96,** 141 (1997).
16. V. V. Kharton, Li Shuangbao, A. V. Kovalevsky, A. P. Viskup, E. N. Naumovich, and A. A. Tonoyan, *Mater. Chem. Phys.* **53,** 6 (1998).
17. J. R. Jurado, F. M. Figueiredo, and J. R. Frade, *Solid State Ionics* **122,** 197 (1999).
18. V. V. Kharton, A. P. Viskup, A. V. Kovalevsky, F. M. Figueiredo, J. R. Jurado, A. A. Yaremchenko, E. N. Naumovich, and J. R. Frade, *J. Mater. Chem.* **10,** 1161 (2000).
19. L. S. M. Traqueia, J. R. Jurado, and J. R. Frade, *in* "Proceedings, International Conference of Electroceramics V" (J. L. Baptista, J. A. Labrincha, and P. M. Vilarinho, Eds.), Vol. 2, p. 151. Aveiro, Portugal, 1996.
20. V. V. Kharton, A. V. Kovalevsky, A. P. Viskup, F. M. Figueiredo, J. R. Frade, A. A. Yaremchenko, and E. N. Naumovich, *Solid State Ionics* **128,** 117 (2000).
21. V. V. Kharton, E. N. Naumovich, A. V. Nikolaev, V. V. Astashko, and A. A. Vecher, *Russ. J. Electrochem.* **29,** 1039 (1993).
22. V. V. Kharton, E. N. Naumovich, A. A. Vecher, and A. V. Nikolaev, *J. Solid State Chem.* **120,** 128 (1995), doi: 10.1006/jssc.1995.1387.
23. A. A. Yaremchenko, V. V. Kharton, A. P. Viskup, E. N. Naumovich, N. M. Lapchuk, and V. N. Tikhonovich, *J. Solid State Chem.* **142,** 325 (1999), doi:10.1006/jssc.1998.8041.
24. H.-H. Moebius, *in* "Extend. Abstr. 37th Meet. ISE," Vol. 1, p. 136. Vilnius, USSR, 1986.
25. S. Steinvik, R. Bugge, J. Gjonnes, J. Tafto, and T. Norby, *J. Phys. Chem. Solids* **6,** 969 (1997).
26. M. Abbate, F. M. F. de Groot, J. C. Fuggle, A. Furimoto, O. Strebel, F. Lopez, M. Domke, G. Kaindl, G. A. Sawadsky, M. Takano, Y. Takeda, H. Eisaki, and S. Uchida, *Phys. Rev. B* **46,** 4511 (1992).
27. R. D. Shannon, *Acta Crystallogr. A* **32,** 751 (1976).
28. T. R. Armstrong, J. W. Stevenson, K. Hasinska, and D. E. McCready, *J. Electrochem. Soc.* **145,** 4282 (1998).
29. J. E. ten Elshof, PhD. thesis, University of Twente, Enschede, The Netherlands, 1997.
30. J.-C. Grenier, N. Ea, M. Pouchard, and P. Hagenmuller, *J. Solid State Chem.* **58,** 243 (1985).
31. A. I. Becerro, C. McCammon, F. Langenhorst, F. Siefert, and R. Angel, *Phase Transitions* **69,** 133 (1999).
32. F. W. Poulsen, G. Lauvstad, and R. Tunold, *Solid State Ionics* **72,** 47 (1994).
33. B. C. H. Steele, *Solid State Ionics* **75,** 157 (1995).
34. S. P. Badwal, *Solid State Ionics* **52,** 23 (1992).
35. A. A. L. Ferreira, J. C. C. Abrantes, J. R. Jurado, and J. R. Frade, *Solid State Ionics*, in press.
36. Y. Takeda, K. Kanno, T. Takada, O. Yamamoto, M. Takano, N. Nakayama, and Y. Bando, *J. Solid State Chem.* **63,** 237 (1986).
37. B. A. van Hassel, T. Kawada, N. Sakai, H. Yokokawa, M. Dokiya, and H. J. M. Bouwmeester, *Solid State Ionics* **66,** 295 (1993).